No. 661   March 2023

Robust adaptive discrete Newton method for regularization-free Bingham model

A. Fatima, M. A. Afaq, S. Turek, A. Ouazzi

Robust adaptive discrete Newton method for regularization-free Bingham model

Arooj Fatima[†,*], Muhammad Aaqib Afaq[†], Stefan Turek[†] and Abderrahim Ouazzi[†]

[†]*Institute for Applied Mathematics, LS III, TU Dortmund University,*
Vogelpothsweg 87, 44227, Dortmund, Germany
[*]*arooj.fatima@math.tu-dortmund.de, aaqib.afaq@math.tu-dortmund.de,*
stefan.turek@math.tu-dortmund.de, abderrahim.ouazzi@math.tu-dortmund.de

Abstract

Developing a numerical and algorithmic tool which accurately detects unyielded regions in yield stress fluid flow is a difficult endeavor. To address these issues, two common approaches are used to handle singular behaviour at the yield surface, i.e. the augmented Lagrangian approach and the regularization approach. Generally, solvers do not operate effectively when the regularization parameter is very small in the regularization approach. In this work, we use a formulation involving a new auxiliary stress tensor, wherein the three-field formulation is equivalent to a regularization-free Bingham formulation. Additionally, a monolithic finite element method is employed to solve the set of equations resulting from the three-field formulation accurately and efficiently, where the velocity, pressure fields are discretized by the higher order stable FEM pair Q_2/P_1^{disc} and the auxiliary stress is discretized by the Q_2 element.

Furthermore, this article presents a novel adaptive discrete Newton method for solving highly nonlinear problems, which exploits the divided difference approach for evaluating the Jacobian. The step size of the solver is dynamically adjusted according to the rate of nonlinear reduction, enabling a robust and efficient approach. Numerical studies of several prototypical Bingham fluid configurations ("viscoplastic fluid flow in a channel", "lid driven cavity" and "rotational Bingham flow in a square reservoir") are used to analyse the performance of this method.

---

1. Introduction

Viscoplastic fluids have been the topic of interest since more than 100 years. These fluids are the prominent part of our daily life e.g. mayonnaise and toothpaste [1]. Apart from the daily life applications, viscoplastic fluid also has high significance in industrial processes e.g. food industry, cosmetic industry, cement industry and the paper making industry. On one hand, the viscoplastic fluids are often considered as highly viscous fluid regime [2] instead of true solid. On the other hand, the clear transition of the rheology from solid to liquid is justified in [3].

It is not possible to accurately predict the solid and liquid regimes of a fluid due to the complex rheological transition such as yield stress fluids, which are the main focus of this work, are particularly dependent on their flow history. These fluids have useful applications in viscoplastic lubrication (hydraulic fracturing) and macro encapsulation [4], such as the transportation of heavy crude oil along pipelines, coal-water slurry transportation and co-extrusion operations. The suppression of interfacial instabilities in multi-layer shear flows [5] and in multiphase flows [6] can be achieved using viscoplastic lubrication.

The threshold value concept of the viscoplastic fluid is reviewed by Barnes et al. [2], accurately knowing or predicting this value for different materials having different properties is really a challenging task. The main difficulty arises because of different regions i.e. rigid zone (fluid moving with uniform velocity) and dead/plug zone (zero velocity region). For acquiring the pre-control of viscoplastic fluids in real life situations, several constitutive models have been proposed. Bingham [7] constitutive model is the most widely used, which includes a discontinuity in the viscosity function, where the shear rate is zero and this discontinuity raises complexities in solving the Bingham model not only analytically but also in the numerically.

In order to circumvent this problem, there are some proposed methods in literature e.g. the augmented Lagrangian method was introduced by Hestenes

2

[8] in 1969 and has been widely used in different studies [9, 10, 11, 12]. Afterwards, Glowinski [13] and Fortin et al. [14] applied it on linear Stokes and nonlinear problems e.g. Bingham fluid flow. The accurate solution of the Bingham fluid is determined by the determination of the yield surfaces, which needs highly refined meshes and are computationally very expensive. One possible remedy was to include a continuous function [13, 14], leading to the idea of the regularization technique [15, 16, 17]. The main advantage of such techniques was "easy numerical implementation". Therefore, a trend of the regularization technique was adopted during 1980's and 1990's. However, in 2001 Samarito et al. [18] again worked on the augmented Lagrangian method to show its accuracy in the prediction of the yielded zones. In consequence, a competition has been developed between regularization and augmented Lagrangian approach. The disadvantage of the later approach is the requirement of the large computation time for complex problems. Whereas, former one is faster for nonlinear complex problems.

2. Mathematical model

Bingham viscoplastic is the limited case of shear thinning fluids, which requires a finite value of the applied stress τ_s before it begins to flow, described by its constitutive law (dependent on the yield stress properties) defined as:

$$
\boldsymbol{\tau} = \begin{cases} 2\eta \mathbf{D}(\boldsymbol{u}) + \tau_s \dfrac{\mathbf{D}(\boldsymbol{u})}{\|\mathbf{D}(\boldsymbol{u})\|} & \text{if } \|\mathbf{D}(\boldsymbol{u})\| \neq 0 \\ \|\boldsymbol{\tau}\| \leq \tau_s & \text{if } \|\mathbf{D}(\boldsymbol{u})\| = 0 \end{cases} \tag{1}
$$

where $\mathbf{D}(\boldsymbol{u}) = \frac{1}{2}(\nabla \boldsymbol{u} + (\nabla \boldsymbol{u})^T)$ denotes the strain rate tensor and τ_s denotes the yield stress. The nonlinear viscosity is defined as:

$$
\eta(\|\mathbf{D}(\boldsymbol{u})\|) = 2\eta + \frac{\tau_s}{\|\mathbf{D}(\boldsymbol{u})\|} \tag{2}
$$

which becomes undefined in the rigid region ($\|\mathbf{D}(\boldsymbol{u})\| = 0$), leading to non-differentiability in the flow domain. In this work, we use a regularization technique based on the Bercovier and Engelman function (eq. 3) to resolve this issue and ensure smoothness of viscosity throughout the domain.

$$
\eta_\epsilon(\|\mathbf{D}(\boldsymbol{u})\|) = 2\eta + \frac{\tau_s}{\sqrt{\epsilon^2 + \|\mathbf{D}(\boldsymbol{u})\|^2}} \tag{3}
$$

3

To numerically approximate these regularized equations, a wide range of iterative solvers can be employed. However, due to the difficulty of obtaining the real viscoplastic solution when the regularization parameter $\epsilon \to 0$, the solvers tend to become inefficient. To counter this challenge, we use a new auxiliary stress tensor $\boldsymbol{\sigma}$ [19] in the formulation, resulting in a regularization-free Bingham model. The three-field $(\boldsymbol{u}, \boldsymbol{\sigma}, p)$ system of stationary Bingham fluid flow equations is given as follows:

$$\begin{cases} \|\mathbf{D}(\boldsymbol{u})\|_\epsilon \boldsymbol{\sigma} - \mathbf{D}(\boldsymbol{u}) = 0 & \text{in } \Omega \\ -\nabla \cdot (2\eta\mathbf{D}(\boldsymbol{u}) + \tau_s\boldsymbol{\sigma}) + \nabla p = 0 & \text{in } \Omega \\ \nabla \cdot \boldsymbol{u} = 0 & \text{in } \Omega \\ \boldsymbol{u} = \boldsymbol{g}_D & \text{on } \Gamma_D \end{cases} \tag{4}$$

where the auxiliary stress tensor $\boldsymbol{\sigma}$ is defined as follows:

$$\boldsymbol{\sigma} = \frac{\mathbf{D}(\boldsymbol{u})}{\|\mathbf{D}(\boldsymbol{u})\|_\epsilon} \tag{5}$$

The system of eq. (4) is a mixed formulation which can be used to solve both the regularized and regularization-free ($\epsilon = 0$) Bingham problem. This formulation not only improves the performance of numerical solvers but also yields an accurate solution, demonstrated by numerical results in the subsequent sections. A monolithic finite element method is employed to solve the set of equations (4), which is converted into the weak formulation, shown in the next section.

3. Weak formulation

We consider three test functions $\boldsymbol{v}, q$ and $\boldsymbol{\tau}$ for velocity, pressure and stress, respectively, and multiply with the system of eq. (4). Then, the resulting weak forms read:

$$\int_\Omega \left(\|\mathbf{D}(\boldsymbol{u})\|_\epsilon \boldsymbol{\sigma} - \mathbf{D}(\boldsymbol{u}) \right) \boldsymbol{\tau} \, dx = 0 \quad \text{in } \Omega$$

$$\int_\Omega \left(-\nabla \cdot \left(2\eta\mathbf{D}(\boldsymbol{u}) + \tau_s\boldsymbol{\sigma} \right) + \nabla p \right) \boldsymbol{v} \, dx = 0 \quad \text{in } \Omega \tag{6}$$

$$\int_\Omega \nabla \cdot \boldsymbol{u} \, q \, dx = 0 \quad \text{in } \Omega$$

4

For simplicity, we consider $u = 0$ at Γ_D and after taking the integration by parts for the second order derivative and the pressure term in the momentum equation, the simplified weak formulation reads:

$$\int_\Omega \left(\|\mathbf{D}(\boldsymbol{u})\|_\epsilon \, \boldsymbol{\sigma} : \boldsymbol{\tau} \right) dx - \int_\Omega \left(\mathbf{D}(\boldsymbol{u}) : \boldsymbol{\tau} \right) dx = 0 \quad \text{in } \Omega$$

$$\int_\Omega \left(2\eta \mathbf{D}(\boldsymbol{u}) : \mathbf{D}(\boldsymbol{v}) \right) dx + \int_\Omega \left(\tau_s \mathbf{D}(\boldsymbol{v}) : \boldsymbol{\sigma} \right) dx - \int_\Omega p \, \nabla \cdot \boldsymbol{v} \, dx = 0 \quad \text{in } \Omega$$

$$\int_\Omega q \, \nabla \cdot \boldsymbol{u} \, dx = 0 \quad \text{in } \Omega$$

$$(7)$$

Let $\mathbb{V} = \boldsymbol{H}_0^1(\Omega) := \left(H_0^1(\Omega)\right)^2$, $\mathbb{Q} = L_0^2(\Omega)$, and $\mathbb{M} = (L^2(\Omega))_{\text{sym}}^{2\times2}$ be the spaces for the velocity, pressure and stress, respectively, associated with $\|.\|_{1,\Omega}$ and $\|.\|_{0,\Omega}$. Let $\mathbb{V}'$, $\mathbb{Q}'$, and $\mathbb{M}'$ be their corresponding dual spaces. Furthermore, we set $\mathbb{X} := \mathbb{V} \times \mathbb{M}$ and $\mathbb{X}' := \mathbb{V}' \times \mathbb{M}'$. We introduce the following linear forms:

$\mathcal{A}_1$ defined on $\mathbb{V} \longrightarrow \mathbb{V}'$

$$\langle \mathcal{A}_1 \boldsymbol{u}, \boldsymbol{v} \rangle := \int_\Omega 2\eta \mathbf{D}(\boldsymbol{u}) : \mathbf{D}(\boldsymbol{v}) \, dx \tag{8}$$

$\mathcal{A}_2$ defined on $\mathbb{M} \longrightarrow \mathbb{M}'$

$$\langle \mathcal{A}_2 \boldsymbol{\sigma}, \boldsymbol{\tau} \rangle = \int_\Omega \tau_s \|\mathbf{D}(\boldsymbol{u})\|_\epsilon \boldsymbol{\sigma} : \boldsymbol{\tau} \, dx \tag{9}$$

The associated bilinear forms $a_1(.,.)$ and $a_2(.,.)$ defined on $\mathbb{V} \longrightarrow \mathbb{V}'$ and $\mathbb{M} \longrightarrow \mathbb{M}'$

$$a_1(\boldsymbol{u}, \boldsymbol{v}) = \langle \mathcal{A}_1 \boldsymbol{u}, \boldsymbol{v} \rangle, \quad a_2(\boldsymbol{\sigma}, \boldsymbol{\tau}) = \langle \mathcal{A}_2 \boldsymbol{\sigma}, \boldsymbol{\tau} \rangle$$

Let B_1 and B_2 defined on $\mathbb{V} \longrightarrow \mathbb{Q}'$ and $\mathbb{V} \longrightarrow \mathbb{M}'$

$$\langle \mathcal{B}_1 \boldsymbol{v}, q \rangle := -\int_\Omega \nabla \cdot \boldsymbol{v} \, q \, dx \quad , \quad \langle \mathcal{B}_2 \boldsymbol{v}, \boldsymbol{\sigma} \rangle := -\int_\Omega \tau_s \mathbf{D}(\boldsymbol{v}) : \boldsymbol{\sigma} \, dx \tag{10}$$

$$\langle \mathcal{A}(\boldsymbol{u}, \boldsymbol{\sigma}), (\boldsymbol{v}, \boldsymbol{\tau}) \rangle = \langle \mathcal{A}_1 \boldsymbol{u}, \boldsymbol{v} \rangle + \langle \mathcal{A}_2 \boldsymbol{\sigma}, \boldsymbol{\tau} \rangle + \langle \mathcal{B}_2^{\mathrm{T}} \boldsymbol{v}, \boldsymbol{\sigma} \rangle + \langle \mathcal{B}_2 \boldsymbol{u}, \boldsymbol{\tau} \rangle$$

The corresponding operator form reads:

$$\begin{bmatrix} \mathcal{A}_1 & \mathcal{B}_2^{\mathrm{T}} & \mathcal{B}_1^{\mathrm{T}} \\ \mathcal{B}_2 & -\mathcal{A}_2 & \mathbf{0} \\ \mathcal{B}_1 & \mathbf{0} & \mathbf{0} \end{bmatrix} \begin{bmatrix} \boldsymbol{u} \\ \boldsymbol{\sigma} \\ p \end{bmatrix} = \begin{bmatrix} rhs_{\boldsymbol{u}} \\ rhs_{\boldsymbol{\sigma}} \\ rhs_p \end{bmatrix}$$

5

The associated bilinear form for $\mathcal{U} = (\boldsymbol{u}, \boldsymbol{\sigma})$ and $\mathcal{V} = (\boldsymbol{v}, \boldsymbol{\tau})$ are

$$a(\mathcal{U}, \mathcal{V}) = a_1(\boldsymbol{u}, \boldsymbol{v}) + a_2(\boldsymbol{\sigma}, \boldsymbol{\tau}) + b_2(\boldsymbol{v}, \boldsymbol{\sigma}) + b_2(\boldsymbol{u}, \boldsymbol{\tau})$$

Find $(\mathcal{U}, p) \in \mathbb{X} \times \mathbb{Q}$ such that:

$$\begin{cases} a(\mathcal{U}, \mathcal{V}) + b(\mathcal{V}, p) = 0 & \forall \mathcal{V} \in \mathbb{X} \\ b(\mathcal{U}, q) \qquad\quad = 0 & \forall q \in \mathbb{Q} \end{cases} \tag{11}$$

3.1. Existence and uniqueness of the solution

In the work of Aposporidis et al. [19], it is shown that the weak formulation of the three-field Bingham (eq. (2.8) of [19]) is equivalent to the weak formulation of the two-field Bingham (eq. (2.4) of [19]) with the regularized viscosity approach. The following theorem states the well-posedness for the weak form of eq. (11)

Theorem 1. *(for proof see [19])*
The mixed formulation has a unique solution $\{\boldsymbol{u}, \boldsymbol{\sigma}, p\}$ from $\boldsymbol{H}_0^1 \times L_{sym}^2 \times L_0^2$ such that

$$\|\boldsymbol{u}\|_1^2 + \epsilon\tau_s \|\boldsymbol{\sigma}\|^2 \leq \|f\|_{-1}, \quad \|p\|_0 + \leq c(\|f\|_{-1} + \tau_s min\{1, \epsilon^{-1} \|f\|_{-1}\}). \tag{12}$$

where ϵ is a regularization parameter and c is a constant. Moreover, $\boldsymbol{\sigma} \in L_{sym}^\infty$ and $\|\boldsymbol{\sigma}\|_{L^\infty} \leq 1$.

There is no extension of this theorem for the well-posedness of regularization-free Bingham case i.e. $\epsilon = 0$. Therefore, It is still an open problem in the theory.

4. Finite element method

FEM finds the approximated solution of the weak problem instead of finding the exact solution of the differential equations (strong form). There are different possible ways for the improvement of the approximated solution e.g. by refining the grid/mesh of the geometry or assuming the higher order polynomials for the interpolation. Let the bounded domain $\Omega \subset \mathbb{R}^d$ be partitioned by a *grid* $\mathcal{T}_h$ consisting of elements $K \in \mathcal{T}_h$ which are assumed

to be open quadrilaterals such that $\Omega = \text{int}\left(\bigcup_{K \in \mathcal{T}_h} \overline{K}\right)$. For an element $K \in \mathcal{T}_h$, we denote by $\mathcal{E}(K)$ the set of all 1-dimensional edges of K. Let $\mathcal{E}_i := \bigcup_{K \in \mathcal{T}_h} \mathcal{E}(K)$ be the set of all interior element edges of the grid $\mathcal{T}_h$. We introduce the approximation spaces as:

$$
\begin{aligned}
\mathbb{V}^h &= \left\{ \boldsymbol{v}_h \in \mathbb{V}, \boldsymbol{v}_{h|K} \in (Q_2(K))^2 \right\} \\
\mathbb{M}^h &= \left\{ \boldsymbol{\tau}_h \in \mathbb{M}, \boldsymbol{\sigma}_{h|K} \in (Q_2(K))^{2 \times 2} \right\} \\
\mathbb{Q}^h &= \left\{ q_h \in \mathbb{Q}, q_{h|K} \in P_1^{\text{disc}}(K) \right\}
\end{aligned}
\tag{13}
$$

The velocity, stress and pressure are discretized using $Q_2, Q_2, P_1^{\text{disc}}$ finite elements, respectively. The approximate discrete problem is now defined as: Find $(\mathcal{U}_h, p_h) \in \mathbb{X}^h \times \mathbb{Q}^h$ such that:

$$
\begin{cases}
a(\mathcal{U}_h, \mathcal{V}_h) + b(\mathcal{V}_h, p_h) = 0 & \forall \mathcal{V}_h \in \mathbb{X}^h \\
b(\mathcal{U}_h, q_h) \hphantom{+ b(\mathcal{V}_h, p_h)} = 0 & \forall q_h \in \mathbb{Q}^h
\end{cases}
\tag{14}
$$

By keeping the test and basis functions same, the discrete formulation will be similar to the system (11) and will provide an approximated solution.

5. Newton method

The three-field Bingham problem (4) is highly nonlinear and poses a challenge for nonlinear solvers. Usually, Newton's method is preferred as a non linear solver due to its faster convergence rate; however, it is sensitive to the initial guess of the solution and relies heavily on the characteristics of the Jacobian matrix during iterations. In order to achieve a fast convergence, not only the initial guess must be close to the final solution; other factors of the Newton method, such as damping factor (when the solution is non-smooth), must also be taken into consideration for numerical stability. In this work, this factor is determined using the line search method [20, 21]. The system of nonlinear equations is linearized using the Newton method, where $\mathcal{U} = (\boldsymbol{u}, \boldsymbol{\sigma}, p)$ and $\mathcal{R}_\mathcal{U}$ denote the discrete residuals. One Newton iteration is as follows:

$$
\begin{bmatrix} \boldsymbol{u}^{n+1} \\ \boldsymbol{\sigma}^{n+1} \\ p^{n+1} \end{bmatrix} = \begin{bmatrix} \boldsymbol{u}^{n} \\ \boldsymbol{\sigma}^{n} \\ p^{n} \end{bmatrix} - \omega_n \begin{bmatrix} \dfrac{\partial R_{\boldsymbol{u}}(\mathcal{U}^n)}{\partial \boldsymbol{u}} & \dfrac{\partial R_{\boldsymbol{u}}(\mathcal{U}^n)}{\partial \boldsymbol{\sigma}} & \dfrac{\partial R_{\boldsymbol{u}}(\mathcal{U}^n)}{\partial p} \\ \dfrac{\partial R_{\boldsymbol{\sigma}}(\mathcal{U}^n)}{\partial \boldsymbol{u}} & \dfrac{\partial R_{\boldsymbol{\sigma}}(\mathcal{U}^n)}{\partial \boldsymbol{\sigma}} & \dfrac{\partial R_{\boldsymbol{\sigma}}(\mathcal{U}^n)}{\partial p} \\ \dfrac{\partial R_{p}(\mathcal{U}^n)}{\partial \boldsymbol{u}} & \dfrac{\partial R_{p}(\mathcal{U}^n)}{\partial \boldsymbol{\sigma}} & \dfrac{\partial R_{p}(\mathcal{U}^n)}{\partial p} \end{bmatrix}^{-1} \begin{bmatrix} \mathcal{R}_{\boldsymbol{u}}(\mathcal{U}^n) \\ \mathcal{R}_{\boldsymbol{\sigma}}(\mathcal{U}^n) \\ \mathcal{R}_{p}(\mathcal{U}^n) \end{bmatrix}
$$

(15)

The Newton method necessitates first derivatives of the residual in each non-linear iteration (Jacobian matrix). Generally, the Jacobian is either determined analytically or approximated via the divided difference approach. The benefit of the latter is its black box nature, which allows for the automatic handling of any nonlinear equation without the need for manual derivation of the calculations [22, 23]. In this work, the Jacobian matrix is approximated using divided differences and the corresponding j-th column is given as follows

$$
\left[\frac{\partial \mathcal{R}(\mathcal{U}^n)}{\partial \mathcal{U}^n} \right]_j \approx \frac{\mathcal{R}(\mathcal{U}^n + \chi \delta_j) - \mathcal{R}(\mathcal{U}^n - \chi \delta_j)}{2\chi}
$$

(16)

here, δ_j is the vector with unit j-th component and zero otherwise, χ is the step size and chosen as a free parameter, the right choice might be a delicate task. Theoretically [24], for double machine precision the value of the $\chi^{\frac{1}{3}} = 10^{-6}$ is suggested but practically, the step size is chosen to be $\chi^{\frac{1}{2}} = 10^{-8}$.

5.1. Bingham viscoplastic fluid flow in a channel

We analyse the solvability of the problem along with the Newton method for Bingham fluids by doing numerical study for this prototypical configuration, where the two dimensional channel is considered as a domain between two parallel plates with unit length apart and long. The following boundary conditions are prescribed on the respective boundary parts [25, 26]:

$$
\begin{aligned}
u_2 &= 0 & &\text{at inflow and outflow} \\
\boldsymbol{u} &= 0 & &\text{at upper and lower walls} \\
\boldsymbol{\tau n.n} &= LC & &\text{at inflow} \\
\boldsymbol{\tau n.n} &= 0 & &\text{at outflow}
\end{aligned}
$$

(17)

where L is the length of the channel (which is unit in our case) and C is the prescribed normal stress, which reduces to pressure in this case, $C = \frac{\partial p}{\partial x} = 1$ and $\boldsymbol{n}$ is the unit normal vector. The analytical solution for the Poiseuille flow in case of Bingham fluid is calculated in [19, 27]. The exact solution for the unit length and width channel reads:

$$
u_1 = \begin{cases} \dfrac{C}{2\eta}y(1-y) - \dfrac{\tau_s}{\eta}y & 0 \le y < \dfrac{1}{2} - \dfrac{\tau_s}{C} \\ \dfrac{C}{2\eta}(\dfrac{1}{2} - \dfrac{\tau_s}{\eta})^2 & \dfrac{1}{2} - \dfrac{\tau_s}{C} \le y \le \dfrac{1}{2} + \dfrac{\tau_s}{C} \\ \dfrac{C}{2\eta}y(1-y) - \dfrac{\tau_s}{\eta}(1-y) & \dfrac{1}{2} + \dfrac{\tau_s}{C} < y \le 1 \end{cases} \tag{18}
$$

$$
p(x, y) = -C(x - L) \tag{19}
$$

A comparison study is carried out for the two-field $(\boldsymbol{u}, p)$ and the three-field $(\boldsymbol{u}, \boldsymbol{\sigma}, p)$ formulation, presented in Table [1], consisting of Newton iterations "NL" and L_2 norm of the velocity error $\|\boldsymbol{u} - \boldsymbol{u}_{ex}\|$.

It can be clearly seen, that the two-field formulation could only solve for non-vanishing regularization parameter up to $\epsilon = 10^{-2}$. On the other hand, the three-field formulation can not only solve very small ϵ but also achieve the goal to solve the regularization-free Bingham $\epsilon = 0$ accurately, quantitatively shown by $\|\boldsymbol{u} - \boldsymbol{u}_{ex}\|$ in Table [1], which assures the true viscoplastic solution. Fig. 2 presents the velocity magnitude for the regularized as well as regularization-free case, as it is already mentioned that the value of the regularization parameter has a great influence on the velocity profile inside the channel domain, therefore the interface of the plug zone is not accurately captured for $\epsilon = 10^{-3}$. On the other hand, when the value of the regularization parameter vanishes (i.e. $\epsilon = 0$), the solution of the velocity in the plug zone perfectly matches with the exact solution shown in Fig. 1. The pressure distribution inside the channel is completely linear throughout the domain based on the Poiseuille theory in the infinite channel. Moreover, the magnitude of the new auxiliary stress tensor shows that the $\|\boldsymbol{\sigma}\| < 1$ in the rigid zone, as expected in this channel flow.

Table 1: **Bingham flow in a channel**: A comparison of the two-field (regularized viscosity approach) $(\boldsymbol{u}, p)$ and three-field $(\boldsymbol{u}, \boldsymbol{\sigma}, p)$ formulations in terms of Newton iterations "NL" and $\|\boldsymbol{u} - \boldsymbol{u}_{ex}\|$ for different mesh refinement levels L and regularization parameter ϵ, with the yield stress value $\tau_s = 0.25$.

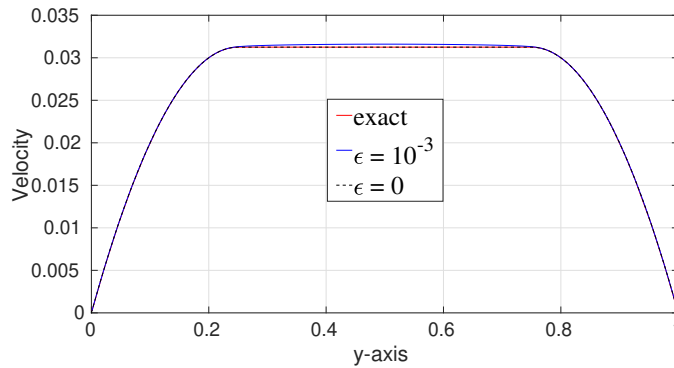|		Two-Field		Three-Field	
ϵ	L	NL	$\|\boldsymbol{u} - \boldsymbol{u}_{ex}\|$	NL	$\|\boldsymbol{u} - \boldsymbol{u}_{ex}\|$
10^{-1}	3	3	3.346×10^{-3}	6	2.598×10^{-3}
	4	3	2.790×10^{-3}	3	2.597×10^{-3}
	5	2	2.563×10^{-3}	2	2.597×10^{-3}
10^{-2}	3	9	1.760×10^{-3}	45	5.873×10^{-4}
	4	6	1.041×10^{-4}	4	5.818×10^{-4}
	5	3	6.771×10^{-4}	3	5.818×10^{-4}
10^{-3}	3	-	-	14	6.257×10^{-5}
	4	-	-	6	6.415×10^{-5}
	5	-	-	4	6.416×10^{-5}
10^{-4}	3	-	-	49	6.407×10^{-6}
	4	-	-	5	6.262×10^{-6}
	5	-	-	4	6.298×10^{-6}
10^{-5}	3	-	-	39	6.788×10^{-7}
	4	-	-	13	6.378×10^{-7}
	5	-	-	5	6.297×10^{-7}
0	3	-	-	18	2×10^{-11}
	4	-	-	4	7×10^{-12}
	5	-	-	3	4×10^{-12}

Figure 1: **Bingham flow in a channel**: Velocity magnitude at $x = 0$ for $\epsilon = 10^{-3}$ and $\epsilon = 0$, plotted with exact velocity profile for $\tau_s = 0.25$.
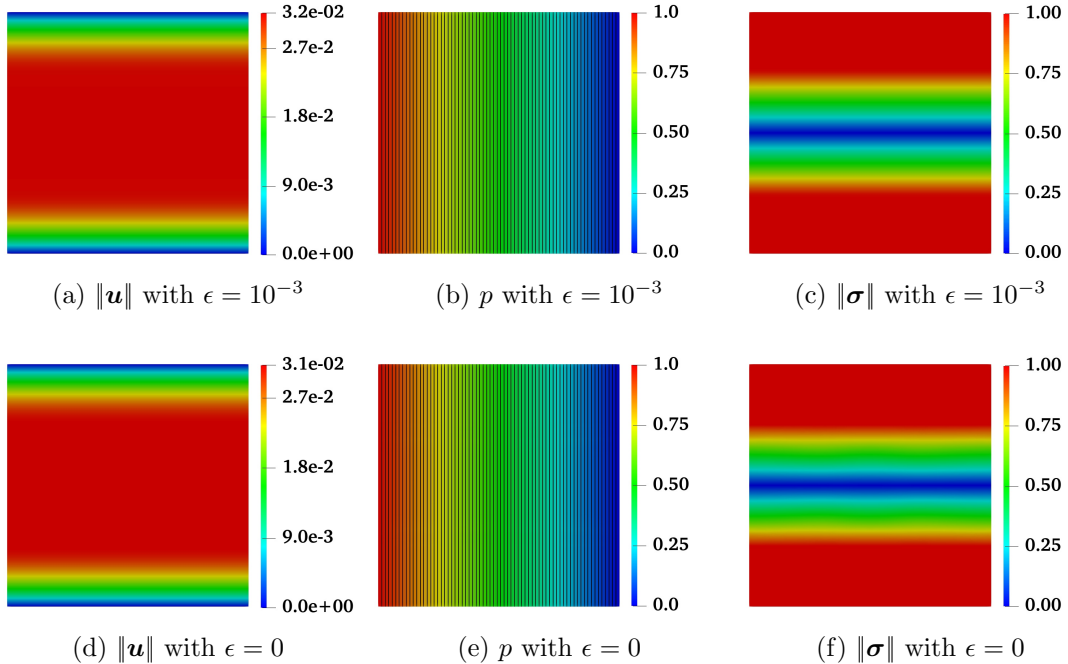
Figure 2: **Bingham flow in a channel**: The visualization of $\|\boldsymbol{u}\|$, p and $\|\boldsymbol{\sigma}\|$ at mesh refinement level 5 ($h = 1/32$) for $\epsilon = 10^{-3}$ (a,b,c) and $\epsilon = 0$ (d,e,f) for system of eq. (4) with $\tau_s = 0.25$.

6. Adaptive discrete Newton

Devoting our attention back to the details of Newton method explained in section 5, which uses the approximated Jacobian matrix, where χ is a free parameter and plays a very important role in the convergence rate of the discrete Newton solver and the choice of the χ is really important because it has a strong impact on the accuracy and robustness of any difference method [24]. Based on the perturbation analysis for the residuum, it can be a fixed constant and often chosen according to the machine precision [28] (corresponds to the Newton method described in section 5). On the other hand, the sensitivity study of the nonlinear behaviour of the Power law models w.r.t. the step size parameter χ, the mesh width h and the strength of the nonlinearity suggests an adaptive choice [29]. Indeed, choosing χ too big leads to the loss of the advantageous quasi-quadratic convergence behaviour

of Newton method. On the contrary, if we choose very small value of χ, the divergence occurs due to the numerical instabilities.

This conclusion lead to the idea of choosing the suitable step size χ adaptively during the approximations. Therefore, a test is performed in [30] for the regularization-free Bingham by changing the step size manually after achieving a certain reduction in the residual $\mathcal{R}(\mathcal{U}^n)$, where two different constant step sizes χ_{c_1} and χ_{c_2} are considered. Initially, the big step size χ_{c_1} is given and after obtaining a certain reduction in the residual, the step size is reduced to the smaller value i.e. χ_{c_2}. The implemented idea of changing the step size between the iterations χ_a produced remarkable results, as the convergence was faster after the χ was changed to χ_{c_2}.

However, to implement this strategy smartly, we allow a process which chooses bigger step size in the start and changes afterwards between the nonlinear iterations. The ratio of the residuum's norm can be used as a step function for the choice of the step size and to relate this ratio continuously to the successive nonlinear reduction, we use a characteristic function introduced in [31] or the slightly modified one in [32] as:

$$f(r_n) = 0.2 + \frac{4.0}{0.7 + \exp\left(1.5 r_n\right)} \tag{20}$$

where

$$r_n = \frac{\|\mathcal{R}(\mathcal{U}^n)\|}{\|\mathcal{R}(\mathcal{U}^{n-1})\|} \tag{21}$$

By doing so, the new strategy uses this function to adapt the step size with the following relation [33]:

$$\chi_{n+1} = f^{-1}(r_n)\chi_n \tag{22}$$

6.1. Bingham viscoplastic fluid flow in a channel

To test the efficiency and robustness of our newly developed adaptive discrete Newton method, a comparison of the new adaptive discrete Newton and the classical Newton for the two and three-field formulation under the same geometry and boundary conditions described in subsection 5.1. The number of nonlinear iterations for each method is shown in Table [2] with the yield stress value $\tau_s = 0.23$, it is observed that the two-field formulation coupled with the classical Newton method had difficulty converging when the

regularization parameter $\epsilon \to 0$. In contrast, the adaptive discrete Newton solver is able to converge even for very small values of ϵ, highlighting the advantages of this newly developed solver. Moreover, the efficiency of the three-field formulation and the robustness of the adaptive strategy are also demonstrated in Table [2], indicating the superiority of this newly developed solver.

Table 2: **Bingham flow in a channel:** Comparison of the Newton and adaptive Newton iterations for the two/three-field formulation at different mesh refinement levels L and regularization parameter ϵ, yield stress $\tau_s = 0.23$.

$\downarrow$ L/ϵ $\rightarrow$	10^{-1}	10^{-2}	10^{-3}	10^{-4}	10^{-5}	0	10^{-1}	10^{-2}	10^{-3}	10^{-4}	10^{-5}	0
			Newton						Adaptive Newton			
Two-Field												
3	2	3	-	-	-	-	4	4	5	5	9	-
4	2	3	-	-	-	-	4	4	5	5	9	-
5	2	3	-	-	-	-	4	4	6	5	9	-
Three-Field												
3	2	3	4	6	9	1	2	2	2	5	1	2
4	2	3	4	8	9	1	1	2	2	4	2	2
5	1	2	3	9	5	2	1	1	1	1	3	1

Furthermore, to highlight robustness of our newly developed solver, a comparison study for different yield stress values τ_s i.e. 0.23, 0.3, 0.4 is carried out, presented in Fig. 3 for mesh refinement levels L=2 and L=3, respectively. All of these tests are carried out for the regularization-free ($\epsilon = 0$) Bingham case, it can be observed in each case of χ_c, the solver either converges very slowly or it starts to oscillate. On the other hand, χ_a is very fast to meet the convergence criteria because initially χ_a is relaxed and once the solution enters the radius of convergence, then the χ_a dynamically changes to achieve the accuracy of the solution. The adaptive discrete Newton solver exhibits the remarkable performance for every τ_s, even for the hardest case (when $\tau_s = 0.4$), where the plug zone covers a very big area in the centre of the channel and the situation becomes very difficult for the fluid to flow.
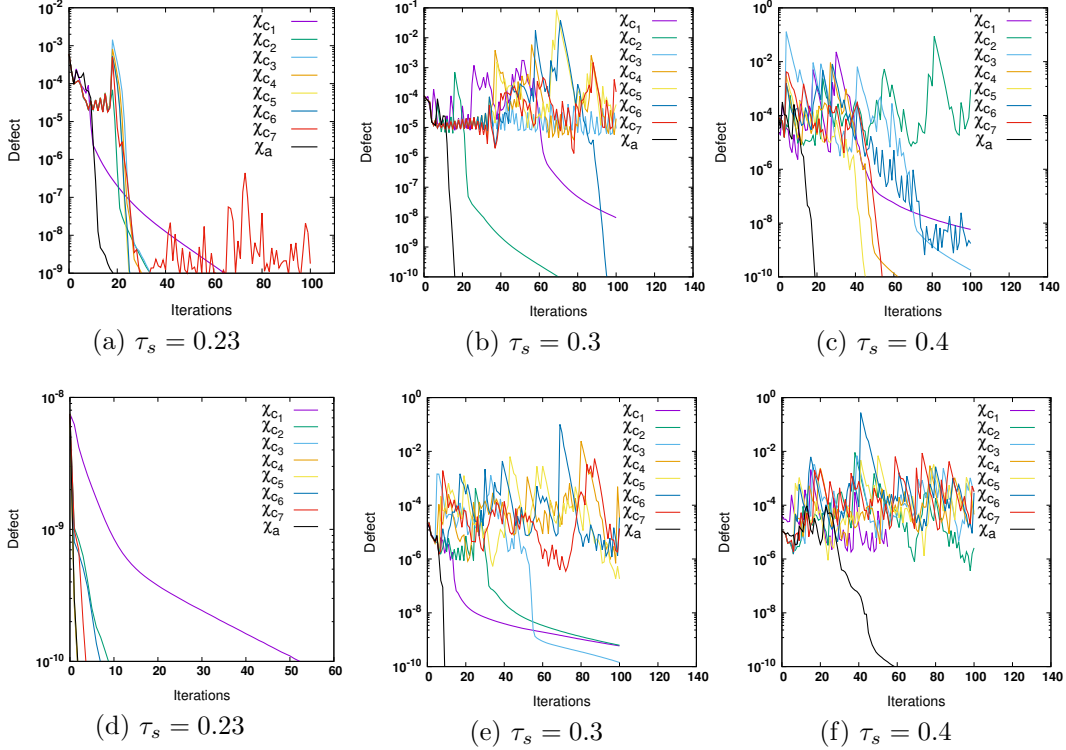
Figure 3: **Nonlinear convergence w.r.t. χ for adaptive Newton method:** The norm of the residual versus number of iterations w.r.t. two strategies (constant (set as $\chi_{c_1} = 10^{-1}, \chi_{c_2} = 10^{-2}, ..., \chi_{c_7} = 10^{-7}$) and adaptive ($\chi_a$)) at refinement level L=2 ($h_x = 1/4, h_y = 1/12$) and L=3 ($h_x = 1/8, h_y = 1/24$) for $\tau_s = 0.23, 0.3, 0.4$.

6.2. Lid-driven cavity

The numerical simulation of Bingham fluid flow for the lid-driven square cavity benchmark is performed for the system of eq. (4). The underlying geometry consists of a unit square domain $\overline{\Omega} = [0,1]^2$. Dirichlet boundary conditions are imposed for $u|_{y=1} = (1,0)^T$ and $u = 0$ everywhere else. The viscosity of the fluid is set to be $\eta = 1$. A validation study for the three-field formulation with the results of [19] is carried out, applying both Newton and the adaptive discrete Newton solver, specifically for the extreme case i.e. regularization-free Bingham, where the yield stress value is set to $\tau_s = 2.0$, shown in Table [3]. Again, the nonlinear iterations of the Newton solver is faster than the Picard's iterative solver (used in the validation study) and the adaptive discrete Newton is the fastest among all.

14

Table 3: **Lid-driven cavity:** Validation of the Newton and adaptive Newton iterations with the Aposporidis et al. [19] for regularization-free ($\epsilon = 0$) Bingham, for the three-field formulation at different mesh refinement levels L, with the yield stress $\tau_s = 2.0$.

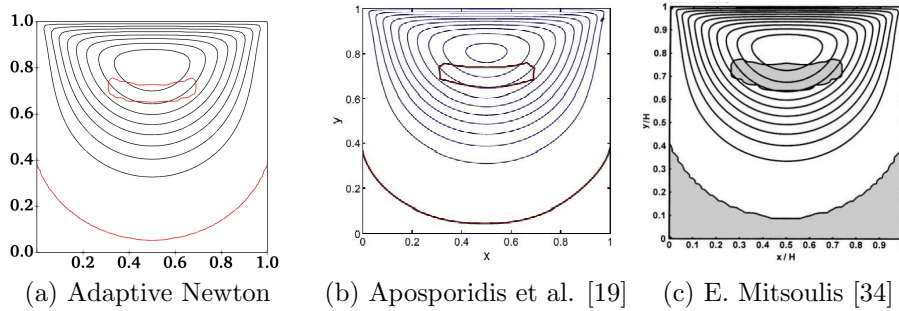| L	Aposporidis et al. [19]	Newton	Adaptive Newton
4	21	13	5
5	23	21	5
6	15	18	6

(a) Adaptive Newton   (b) Aposporidis et al. [19]   (c) E. Mitsoulis [34]

Figure 4: **Lid-driven cavity:** The superposition of unyielded zones on the streamline contours for the regularization-free ($\epsilon = 0$) Bingham, for the three-field formulation at mesh refinement levels L=6 (h=1/64), where the yield stress is set to $\tau_s = 2.0$.

The accuracy of the solution in terms of validation is presented in Fig. 4, shows a good agreement with the results of [19] and [34]. Fig. 5 illustrates the efficiency of the adaptive discrete Newton solver for both values of τ_s for the regularization-free Bingham, as it converges in very less number of iterations. On the other hand, the constant step size either oscillates or converges very slowly. In order to test the limit of the complexity handled by the adaptive discrete Newton, in terms of the threshold value τ_s of Bingham fluid. The forthcoming tests are carried out by increasing the value of τ_s, given in Table [4]. The adaptive discrete Newton shows faster convergence with significantly less number of nonlinear iterations. The effect of increasing the τ_s on the growth of dead zones in the cavity can be seen very clearly in Fig. 6, where the unyielded zones grows significantly (which increases the no flow area (shaded in black)). This implies that the adaptive discrete Newton solver is not only efficient but also solves accurately by predicting the accurate unyielded zones.
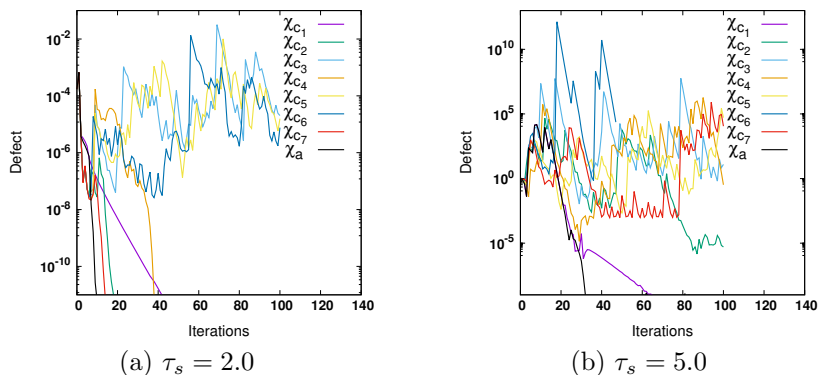
15

(a) $\tau_s = 2.0$ (b) $\tau_s = 5.0$

Figure 5: **Nonlinear convergence w.r.t χ for adaptive discrete Newton method**: The norm of the residual versus number of iterations w.r.t. two strategies (constant and adaptive) at refinement level L=4 ($h_x = 1/16, h_y = 1/16$) for τ_s 2.0 and 5.0.

Table 4: **Lid-driven cavity:** Summary of the adaptive discrete Newton iterations for the three-field formulation, for different yield stress values at different refinement levels L, for regularization-free ($\epsilon = 0$) Bingham.

$\downarrow$ L/τ_s $\rightarrow$	2	5	7.5	10	15	20	40	50
3	5	5	2	101	79	3	8	18
4	5	6	6	4	5	5	6	7
5	6	6	2	3	5	5	6	9

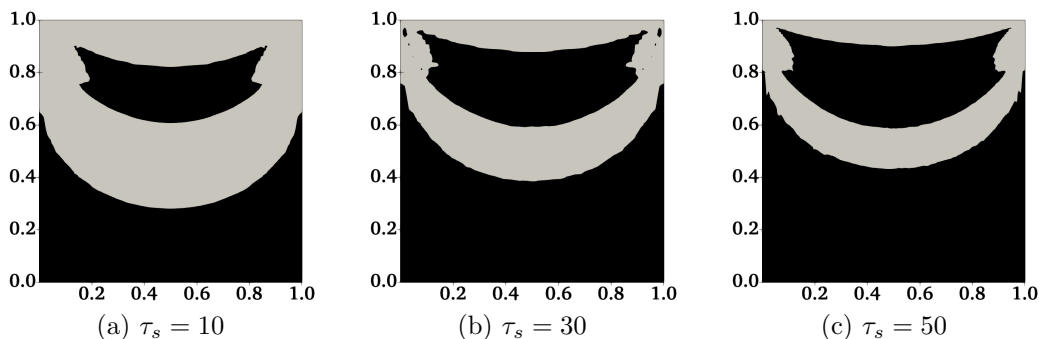(a) $\tau_s = 10$ (b) $\tau_s = 30$ (c) $\tau_s = 50$

Figure 6: **Unyielded zones:** The unyielded zones of the regularization-free ($\epsilon = 0$) Bingham for different yield stress values $\tau_s = 10, 30, 50$ at refinement level L=5 ($h = 1/32$).

16

6.3. Rotational Bingham flow in a square reservoir

In this section, a numerical study of the rotational Bingham flow in a square reservoir benchmark [35, 36] is carried out, specifically for the regularization-free ($\epsilon = 0$) case. This configuration should produce the true viscoplastic solution of the problem. The benchmark is validated with a recent numerical results presented in [36]. The configuration settings includes a wall driven force $\boldsymbol{f}$ described as:

$$\boldsymbol{f}(x_1, x_2) = 300 \left(x_2 - 0.5, 0.5 - x_1 \right)$$

over the domain $\Omega = [0, 1]^2$ with the yield stress value $\tau_s = 14.5$. In this numerical experiment, the flow behaviour is analysed with the motion on the boundaries.

(a) Velocity field   (b) Velocity field [36]

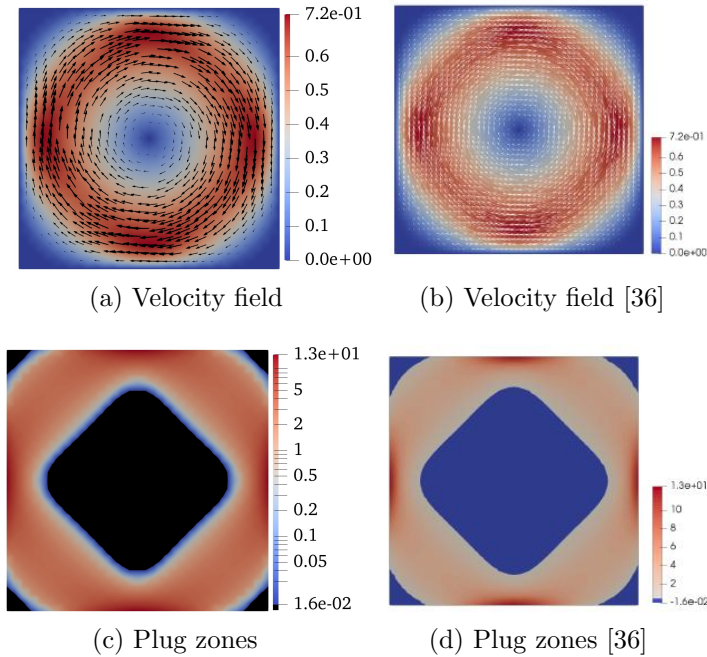(c) Plug zones   (d) Plug zones [36]

Figure 7: **Bingham flow in a square reservoir:** Velocity field (a,b) and plug zones (c,d) of regularization-free ($\epsilon = 0$) Bingham at mesh refinement level L=5 for yield stress value $\tau_s = 14.5$.

Fig. 7 presents the validation in terms of the velocity field and the plug zones prediction, respectively. A central solid rigid zone is expected as a true

solution of the Bingham viscoplastic fluid in this application. Our results are in good agreement for the velocity field Fig. 7 (a) as well as for the calculation of the unyielded zones Fig. 7 (c). This assures the accuracy and the efficiency of our monolithic solver with adaptive discrete Newton method for regularization-free Bingham model.

7. Conclusions

In this work, a three-field regularization-free Bingham solver and a new adaptive discrete Newton solver for the simulation of viscoplastic flows have been developed. This formulation uses an auxiliary stress tensor, enabling a true regularization-free viscoplastic solution, and thus, does not alter the shape of the yield surfaces. Furthermore, the adaptive discrete Newton method changes the step size very intelligently in the evaluation of the Jacobian matrix with the divided difference approach, which is more efficient and accurate than the classical Newton. Through numerical studies of several benchmark problems, this method provides an efficient and robust monolithic solver for Bingham fluid flow problems. Additionally, the adaptive discrete Newton solver can be applied to other nonlinear problems due to its capability of handling any nonlinearity of the system of equations and providing a fast speed of convergence with an accurate solution.

References

[1] P. Coussot, Yield stress fluid flows: A review of experimental data, Journal of Non-Newtonian Fluid Mechanics 211 (2014) 31–49.

[2] H. A. Barnes, K. Walters, The yield stress myth?, Rheologica Acta 24 (1985) 323–326.

[3] G. Astarita, Letter to the editor: The engineering reality of the yield stress, Journal of Rheology 34 (1990) 275–277.

[4] A. Maleki, S. Hormozi, A. Roustaei, I. A. Frigaard, Macro-size drop encapsulation, Journal of Fluid Mechanics 769 (2015) 482–521.

[5] P. Sarmadi, O. Mierka, S. Turek, S. Hormozi, I. A. Frigaard, Three dimensional simulation of flow development of triple-layer lubricated pipeline transport, Journal of Non-Newtonian Fluid Mechanics 274 (2019) 104201.

[6] M. A. Afaq, S. Turek, A. Ouazzi, A. Fatima, Monolithic Newton-multigrid solver for multiphase flow problems with surface tension, in: Book of Extended Abstracts of the 6th ECCOMAS Young Investigators Conference 7th-9th July 2021, Valencia, Spain, Editorial Universitat Politècnica de València, 2021, pp. 190–199. doi:https://doi.org/10.4995/YIC2021.2021.12390.

[7] E. C. Bingham, Fluidity and plasticty, International chemical series, 1st ed., McGraw-Hill Book Company, inc., 1922.

[8] M. R. Hestenes, Multiplier and gradient methods, Journal of Optimization Theory and Applications 4 (1969) 303–320.

[9] R. R. Huilgol, M. P. Panizza, On the determination of the plug flow region in Bingham fluids through the application of variational inequalities, Journal of Non-Newtonian Fluid Mechanics 58 (1995) 207–217.

[10] R. Huilgol, Z. You, Application of the augmented lagrangian method to steady pipe flows of Bingham, Casson and Herschel–Bulkley fluids, Journal of Non-Newtonian Fluid Mechanics 128 (2005) 126–143.

[11] P. Saramito, N. Roquet, An adaptive finite element method for viscoplastic fluid flows in pipes, Computer Methods in Applied Mechanics and Engineering 190 (2001) 5391–5412.

[12] R. Glowinski, Approximation of a Bingham-type elliptic, variational inequality, Rev Fr Autom Inf Rech Oper 10 (1976) 13–30.

[13] R. Glowinski, Lectures on numerical methods for non-linear variational problems, Springer Science & Business Media, 2008.

[14] M. Fortin, R. Glowinski, Augmented Lagrangian methods : Applications to the numerical solution of boundary-value problems, Elsevier Science Pub. Co., 1983.

[15] E. Dean, R. Glowinski, G. Guidoboni, On the numerical simulation of bingham visco-plastic flow: Old and new results, Journal of Non-Newtonian Fluid Mechanics 142 (2007) 36–62.

[16] M. Bercovier, M. Engelman, A finite-element method for incompressible non-Newtonian flows, Journal of Computational Physics 36 (1980) 313–326.

[17] T. C. Papanastasiou, Flows of materials with yield, Journal of Rheology 31 (1987) 385–404.

[18] N. Roquet, P. Saramito, An adaptive finite element method for Bingham fluid flows around a cylinder, Computer Methods in Applied Mechanics and Engineering 192 (2003) 3317–3341.

[19] A. Aposporidis, E. Haber, M. Olshanskii, A. Veneziani, A mixed formulation of the Bingham fluid flow problem: Analysis and numerical solution, Computer Methods in Applied Mechanics and Engineering 200 (2011) 2434–2446.

[20] J. E. Dennis, R. B. Schnabel, Numerical Methods for Unconstrained Optimization and Nonlinear Equations, Society for Industrial and Applied Mathematics, 1996. doi:10.1137/1.9781611971200.

[21] W. H. Press, S. A. Teukolsky, W. T. Vetterling, B. P. Flannery, Numerical Recipes in C++: The Art of Scientific Computing, Cambridge University Press, 2002.

[22] H. Damanik, FEM Simulation of Non-isothermal Viscoelastic Fluids, TU Dortmund, Germany, 2011. PhD Thesis.

[23] H. Damanik, J. Hron, A. Ouazzi, S. Turek, Monolithic Newton-multigrid solution techniques for incompressible nonlinear flow models, International Journal for Numerical Methods in Fluids 71 (2012) 208–222.

[24] H.-B. An, J. Wen, T. Feng, On finite difference approximation of a matrix-vector product in the Jacobian-free Newton–krylov method,

Journal of Computational and Applied Mathematics 236 (2011) 1399–1409.

[25] J. Málek, V. Průša, K. R. Rajagopal, Generalizations of the Navier–Stokes fluid from a new perspective, International Journal of Engineering Science 48 (2010) 1907–1924.

[26] J. Hron, J. Málek, J. Stebel, K. Touska, A novel view on computations of steadyflows of Bingham fluids using implicit constitutive relations (2017).

[27] M. El-Borhamy, Numerical Simulation for viscoplastic fluids via finite element methods, TU Dortmund, Germany, 2012. PhD Thesis.

[28] C. T. Kelley, Iterative methods for linear and nonlinear equations, SIAM, Philadelphia, 1995.

[29] J. Hron, A. Ouazzi, S. Turek, A computational comparison of two FEM solvers for nonlinear incompressible flow, in: Lecture Notes in Computational Science and Engineering, volume 35, Springer, 2003, pp. 87–109. New York.

[30] A. Fatima, An adaptive discrete Newton method for regularization-free Bingham model, TU Dortmund, Germany, 2023. PhD Thesis.

[31] S. Mandal, A. Ouazzi, S. Turek, Modified Newton solver for yield stress fluids, in: Proceedings of ENUMATH 2015, the 11th European Conference on Numerical Mathematics and Advanced Applications, Springer, 2016, pp. 481–490.

[32] S. Mandal, Efficient FEM solver for quasi-Newtonian flow problems with application to granular material, TU Dortmund, Germany, 2016. PhD Thesis.

[33] A. Fatima, S. Turek, A. Ouazzi, M. A. Afaq, An adaptive discrete Newton method for regularization-free Bingham model, in: Book of Extended Abstracts of the 6th ECCOMAS Young Investigators Conference 7th-9th July 2021, Valencia, Spain, Editorial Universitat Politècnica de València, 2021, pp. 180–189. doi:https://doi.org/10.4995/YIC2021.2021.12389.

[34] E. Mitsoulis, T. Zisis, Flow of Bingham plastics in a lid-driven square cavity, Journal of Non-newtonian Fluid Mechanics 101 (2001) 173–180.

[35] J. C. D. L. Reyes, S. G. Andrade, A combined BDF-semismooth Newton approach for time-dependent Bingham flow, Humboldt-Universität zu Berlin, Mathematisch-Naturwissenschaftliche Fakultät II, Institut für Mathematik, 2011. doi:http://dx.doi.org/10.18452/2817.

[36] S. González, S. López, P. Merino, Nonsmooth exact penalization second-order methods for incompressible Bingham flows (2020).